Single Antibody Detection in a DNA Origami Nanoantenna

Martina Pfeiffer [1†*], Kateryna Trofymchuk [1†*], Simona Ranallo [2], Francesco Ricci [2], Viktorija Glembockyte [1*] and Philip Tinnefeld [1*]

[1] Department of Chemistry and Center for NanoScience, Ludwig-Maximilians-Universität München, Butenandtstr. 5-13, 81377 München, Germany

[2] Department of Chemistry of Rome, Tor Vergata, Via della Ricerca Scientifica, 00133 Rome, Italy

† These authors contributed equally

* email: martina.pfeiffer@cup.lmu.de; kateryna.trofymchuk@cup.lmu.de; viktorija.glembockyte@cup.lmu.de; philip.tinnefeld@cup.uni-muenchen.de

Summary

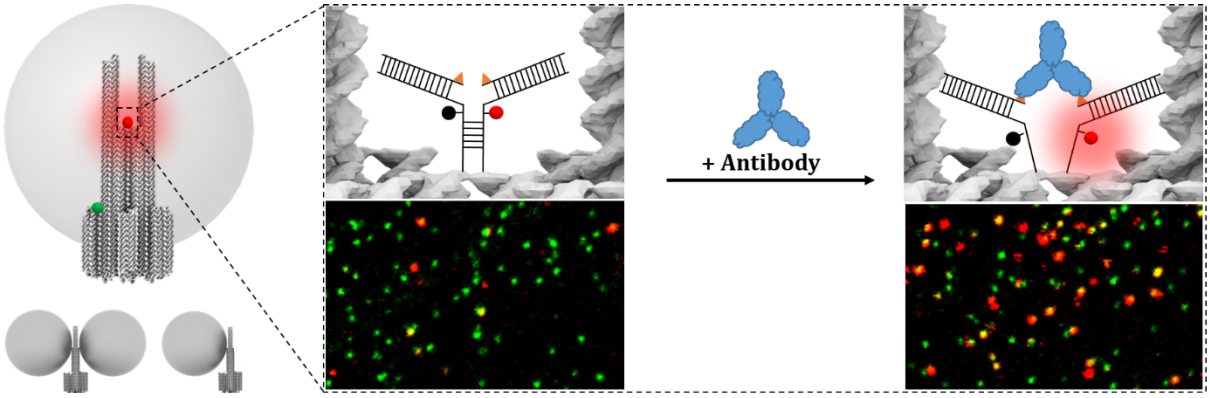

DNA nanotechnology offers new biosensing approaches by templating different sensor and transducer components. Here we combine DNA origami nanoantennas with label-free antibody detection by incorporating a nanoswitch in the plasmonic hotspot of the nanoantenna. The nanoswitch contains two antigens that are displaced by antibody binding thereby eliciting a fluorescent signal. Single antibody detection with a dig antibody nanoswitch is demonstrated with a DNA origami integrated nanoswitch. In combination with the nanoantenna, the signal generated by the antibody is additionally amplified. Overall, fluorescence enhanced antibody detection in DNA origami nanoantennas shows that fluorescence enhanced biosensing can be expanded beyond the scope of the nucleic acids realm.

Introduction

Over the last decades, DNA nanotechnology and in particular the DNA origami technique have emerged as an indispensable tool for designing new biosensors on the nanoscale. As introduced by Rothemund, (Rothemund et al., 2006) DNA origami can be used to fabricate various two- or three-dimensional shapes using a long single-stranded scaffold (about 7000 – 8000 nucleotides (nt)) and hundreds of short staple strands (about 40 nt). Utilizing the programmable nature of DNA base pairing and functionalized staple strands, a large number of different functionalities can be introduced on the nanoscale. This unprecedented addressability of the DNA origami approach allows arranging different biosensing components, introducing new biorecognition elements and multiplexing strategies, as well as implementation of signal transduction and amplifications mechanisms. Using DNA origami, a number of biosensors have been developed capable of single-molecule detection of DNA and RNA (Zhang et al., 2010a, Ochmann et al., 2017, Trofymchuk et al., 2021, Selnihhin et al., 2018, Kuzuya et al., 2011, Funck et al., 2018, Ke et al., 2008), single nucleotide polymorphisms (Zhang et al., 2010b, Subramanian et al., 2011), specific metal ions (Ke et al., 2008), as well as various protein biomarkers (Raveendran et al., 2020, Godonoga et al., 2016, Koirala et al., 2014, Rinker et al., 2008) among many others (Wang et al., 2017b, Wang et al., 2020, Chandrasekaran, 2017, Loretan et al., 2020, Wang et al., 2017a, Dass et al., 2021, Ke et al., 2018).

Nevertheless, the use of these biosensors is often limited to the detection of targets that directly interact with DNA (e.g. nucleic acids or proteins with aptameric targets). The methods that are used to detect the analyte-sensor interactions also often require low-throughput, complex analytical techniques, such as atomic force microscopy, limiting the wide-spread application of DNA origami biosensors in clinical diagnostics. Recent advances in the development of high-throughput DNA origami-enabled optical (Domljanovic et al., 2017, Funck et al., 2018) or nanopore-based (Keyser, 2016, Raveendran et al., 2020) sensing strategies provide excellent examples of how to bridge this gap. However, general strategies on how to incorporate recognition elements for targets that go beyond nucleic acids (such as antibodies) are still highly sought after (Wang et al., 2017b).

Due to its quick response, high contrast and good sensitivity, fluorescence provides a powerful readout strategy for developing such sensing devices. Using the DNA origami approach, one can also incorporate methods to further amplify the fluorescence response (Wang et al., 2017a). This enables the detection of single target molecules on low-cost optical devices (Trofymchuk et al., 2021). A way to enhance the fluorescence intensity of a molecule is to put it in a higher electric field environment, which for example is created close to the surface of plasmonic silver (Ag) or gold (Au) nanoparticles (NPs) upon their illumination(Novotny and van Hulst, 2011, Purcell E.M., 1946). Even higher electric field enhancement can be achieved in a gap (plasmonic hotspot) between two plasmonic NPs(Li et al., 2003). Our group has explored this

signal amplification strategy to design light antennas on the nanoscale (Acuna et al., 2012, Puchkova et al., 2015, Vietz et al., 2017a) that can be used to amplify the signal of molecular assays (Ochmann et al., 2017, Trofymchuk et al., 2021). In this context, the strength of DNA nanotechnology compared to other approaches of creating plasmonic fluorescence enhancement is the possibility of targeted placement of nanoparticles and fluorescence enhancement with respect to each other. First, we showed that the detection of DNA and RNA specific to Zika virus can be achieved with a fluorescence-quenched hairpin based assay when positioned next to a plasmonic AgNP, allowing for around 7-fold average fluorescence enhancement (Ochmann et al., 2017). More recently, the challenge that plasmonic hotspots in gap nanoantennas with gap sizes of the order of 10-20 nm are ultimately small was tackled by DNA origami nanoantennas with cleared hotspot (NACHOS)(Trofymchuk et al., 2021), which allowed positioning a DNA detection assay in the hotspot of two AgNPs enabling an average fluorescence enhancement of 90-fold and the detection of single target molecules on a low-cost, portable, and battery-driven smartphone device.

Here, we address the question whether DNA origami nanoantennas could be applied to larger structures beyond the realm of nucleic acids, such as antibodies. Development of specific recognition elements capable of eliciting a signal response upon binding of other non-labeled biomolecular targets, including antibodies, could provide means to expand the utility of the DNA nanoantenna as well as other DNA-origami based sensors for a wider range of targets and diagnostic applications. A promising strategy to combine the specific recognition of antibody targets with DNA-based biosensors that relies on a DNA nanoswitch has been developed recently (Ranallo et al., 2015, Porchetta et al., 2018). DNA containing a fluorophore-quencher pair is used as a scaffold to attach specific recognition elements and transduce target detection through fluorescence output. In absence of an antibody target, the nanoswitch adopts a stem-loop conformation that opens upon binding to the antibody target, separating the fluorophore and the quencher pair and resulting in a fluorescence signal. With this nanoswitch design, two different antibody targets were simultaneously detected and the dynamic range of the response could be tuned. Also, nanomolar sensing capabilities with rapid response times were demonstrated.

In this work, we report a single-molecule DNA origami-based sensor for antibodies by incorporating nanoswitch recognition elements into DNA origami nanostructures. First, we demonstrate the feasibility of this sensor strategy on a simple new rectangular DNA origami (NRO) structure (Rothemund, 2006, Woo and Rothemund, 2011, Li et al., 2012), showing the specific detection of anti-Dig antibodies at sub-nanomolar concentrations within few minutes. We then incorporate the nanoswitch elements in the hotspot of DNA nanoantennas showing that the signal of the nanosensor can be enhanced up to several tenfold. The single-molecule sensing platform reported here allows to increase the limit of detection of the nanoswitch and combine it with signal

amplification strategies. Additionally, the modular nature of the DNA origami approach opens exciting possibilities for even further multiplexing in rapid antibody detection.

Results

Detection of anti-Dig antibodies with a nanoswitch on the NRO at the single-molecule level

To demonstrate a direct detection of antibodies on DNA origami at the single-molecule level, the new rectangular DNA origami (NRO) was chosen as a model structure. A simple two-dimensional shape of NRO provides an ideal platform to incorporate antibody sensing units with high accessibility (Figure 1a). A sensing unit, which is inspired by the nanoswitch sensor for antibodies developed by Ricci group (Ronallo et al., 2015), was incorporated into the NRO structure during DNA origami folding process. The nanoswitch consists of two single-stranded (ss)DNA strands protruding from the NRO nanostructure with their 3'- and 5'-ends. Both strands contain a 7-nt long, non-complementary linker sequence followed by a 5-nt long complementary sequence which forms a stem (Figure 1a). The stem is modified on one ssDNA strand with ATTO647N and on the other ssDNA strand with BlackBerry Quencher 650 which form a dye-quencher pair. The stem is followed by a DNA anchors on both strands. The DNA anchors allow hybridizing two digoxigenin (Dig)-modified ssDNA strands which provide binding sites for Dig binding antibodies. Each NRO nanostructure is equipped with six biotinylated DNA strands for surface immobilization on BSA-biotin-neutravidin coated glass coverslips. Additionally, to aid identifying each DNA origami nanosensor in the single-molecule fluorescence experiments, a green-absorbing ATTO542 dye is incorporated in the NRO nanostructure (Figure 1a).

The principle of the nanoswitch is illustrated in Figure 1a. In the absence of target molecules, the stem is closed and the dye-quencher pair is in close proximity so that the fluorescence of the ATTO 647N dye is quenched. Bivalent binding of anti-Dig antibodies to the Dig-recognition elements opens the stem and separates fluorophore and quencher spatially. This results in a fluorescence increase of ATTO 647N. The binding of the antibody can be detected in single-molecule confocal fluorescence images (Figure 1b) where red-green colocalized spots are attributed to DNA origami structures with an opened nanoswitches whereas only green spots indicate the presence of structures with closed nanoswitches.

Upon antibody binding, the chosen 7-nt long linker and the 5-nt long stem provide a 26-nt long ssDNA spacer between the two Dig-moieties. This spacer length and design is comparable to the 27-nt long ssDNA spacer in the original nanoswitch design ((Ranallo et al., 2015)) and is consistent with the optimal ~ 16 nm distance between two Dig binding moieties on DNA origami recently reported (Shaw et al., 2019).

To test the specificity of the nanoswitch opening on NRO and to investigate the opening mechanism, we studied nanoswitch constructs bearing one, two or no Dig recognition elements**.** After surface immobilization, fluorescence scans of the three constructs were taken before and after 20 min incubation with 100 nM anti-Dig antibody on a confocal fluorescence microscope (Figure 1b-d). For all three constructs, surface scans before incubation with the target antibody show very few co-localized spots indicating only a low fraction of opened nanoswitches. This small number of false positive signals might originate from unspecifically opened nanoswitches, mislabeled nanoswitches (structures where the quencher was not incorporated), or nanoswitches containing a photobleached BBQ650 quencher (Holzmeister et al., 2014, Grabenhorst

et al., 2020). After incubating the different nanoswitch constructs with anti-Dig antibodies, we only noted a significant increase of co-localized spots for the nanoswitch construct bearing two Dig recognition elements (Figure 1b-e). This confirms the specific nature of antibody binding to the Dig recognition elements and excludes an opening of the nanoswitch by monovalent binding of one anti-Dig antibody.

To quantify the efficiency of the nanoswitch opening, we calculated the fraction of NRO nanostructures with an opened nanoswitch (fraction of co-localized green and red spots, Figure 1f). For the construct bearing two Dig-recognition elements, the percentage of constructs with opened nanoswitches increased from ~5% to ~54% upon addition of anti-Dig antibody while no significant increase was observed for both other constructs, demonstrating specific binding of the anti-Dig antibody to the Dig recognition elements.

To further investigate the opening mechanism and exclude possible cross-reactivity with other bivalent binding antibodies, we incubated the nanoswitch construct with 100 nM anti-Dig Fab fragment and 100 nM anti-hDectin-1 antibody (see Figure 1e). The anti-Dig Fab fragment is a monovalent Dig-binding protein and thus can be used to exclude an opening of the nanoswitch by monovalent binding of two antibodies. We observed only a slight increase (~4%) in the fraction of opened nanoswitches upon addition of the anti-Dig Fab (see Figure 1f), supporting the assumption that the nanoswitch is opened due to the bivalent binding of an anti-Dig antibody which is consistent with the mechanism proposed by Ranallo et al. (Ranallo et al., 2015). Anti-hDectin1 is a bivalent antibody specific for human Dectin-1. The nanoswitch opening in presence of anti-hDectin-1 antibodies (5%) (Figure 2f) is comparable to the unspecific signal gain, further demonstrating that no cross-reactivity occurs. All in all, these control experiments confirmed that the nanoswitch is specific for the target anti-Dig antibody and works according to the mechanism depicted in Figure 1a.

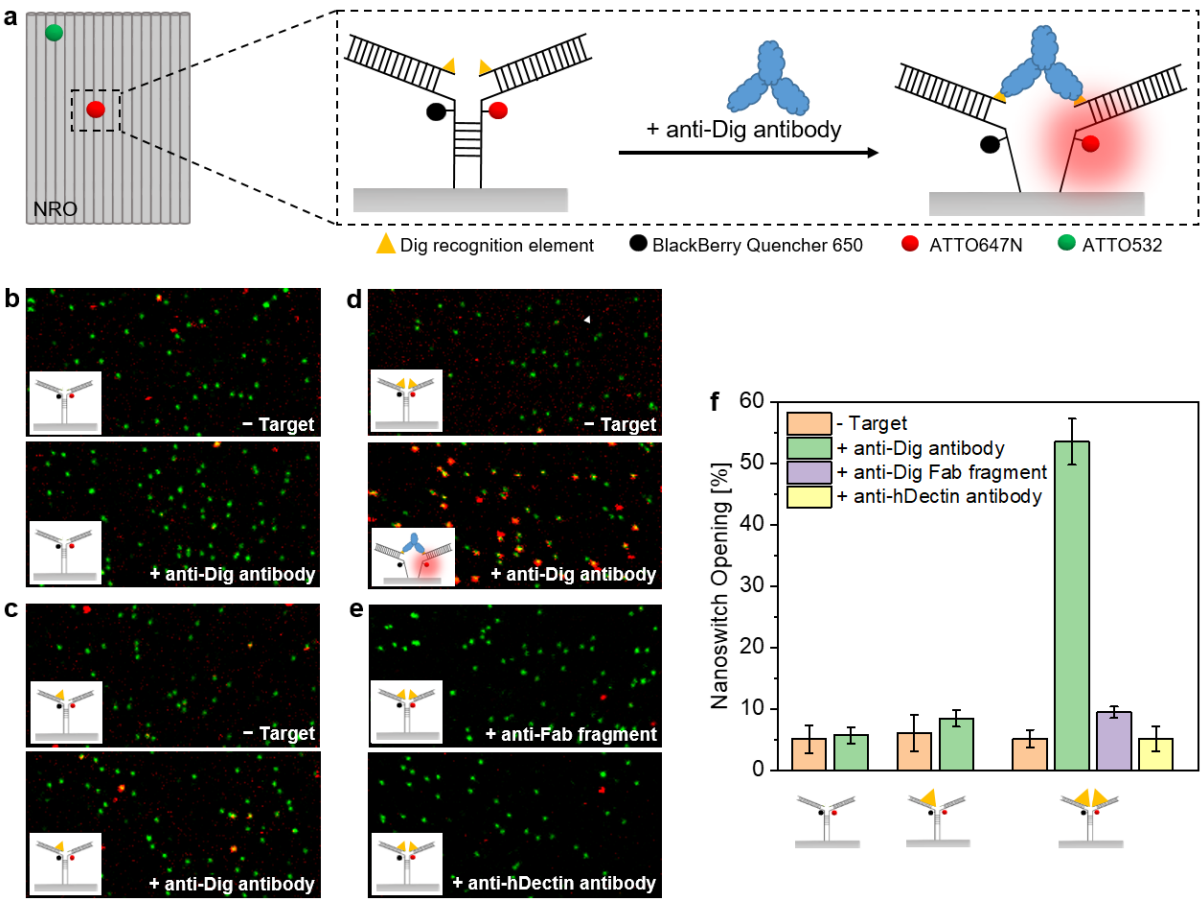

Figure 1. Detection of anti-Dig antibodies with a nanoswitch on the NRO at the single-molecule level. (a) Schematic representation of a NRO nanostructure with an incorporated nanoswitch (dimensions are not to scale). The nanoswitch consists of two DNA strands protruding from the NRO with their 3' and 5' ends. Both strands contain a 7-nt long, non-complementary linker sequence followed by a 5-nt long stem. The stem is modified with a dye (ATTO647N)-quencher (BlackBerry Quencher 650) pair and followed by a ssDNA anchor on both strands. The DNA anchors allow hybridizing two digoxigenin (Dig)-modified ssDNA strands which form binding sites for Dig binding antibodies to the nanoswitch. In absence of target molecules, the stem is closed and an efficient energy transfer from the fluorophore to the quencher occurs due to their close proximity. Upon bivalent binding of an antibody to the Dig recognition elements, fluorophore and the quencher pair is separated and the fluorescence signal of ATTO647N is increased. To localize the DNA origami structure, a green-absorbing ATTO 532 dye is incorporated. To test the specificity of the nanoswitch opening and the opening mechanism of the nanoswitch three different nanoswitch constructs bearing different numbers (0, 1, 2) of Dig recognition elements were investigated. (b-d) Two-color fluorescence confocal images of surface immobilized NRO-nanoswitch constructs bearing zero Dig recognition elements, one Dig recognition element, and two Dig recognition elements before and after 20 min incubation with 100 nM anti-Dig antibodies. (e) Two-color fluorescence images of surface immobilized NRO-nanoswitch constructs bearing two Dig recognition elements after incubation with 100 nM anti-Dig Fab fragment (left) and anti-h-Dectin antibodies (right), respectively. The images show a field of view of 20 µm x 10 µm. Co-localized green and red spots are attributed to functional NRO structures with an open nanoswitch. (c) The fraction of open nanoswitches was quantified for every sample by dividing the number of green and red co-localized spots by the total number of all green spots from fluorescence confocal scans. Over 300 structures from 5 different areas per sample were analyzed. Error bars represent the standard deviation of the 5 areas.

Enhancing the output signal of the nanoswitch in the plasmonic hotspot of nanoantennas

To provide physical amplification of the signal upon detection of a single antibody, we utilized recently developed NACHOS. NACHOS use a three-dimensional DNA origami structure consisting of two pillars each bearing six protruding staple strands (A20) which provide anchor points for 100-nm Ag NPs functionalized with ssDNA strands

(T20) (Figure 2a). A plasmonic hotspot is created at the bifurcation in the gap between the two pillars and the nanoparticle (see DNA origami sketch and TEM image in Figure 2a (left) and full NACHOS structure in Figure 2a (right)). For immobilization on a BSA-biotin-neutravidin coated glass coverslips, the DNA origami structure is equipped with a rigid cross-like shaped base (Supplementary Figure 2 and 3) that contains six biotin-modified staple strands. For identifying NACHOS in single-molecule fluorescence images, a reference green-absorbing dye ATTO542 is incorporated at the base of the DNA origami structure.

To study the possible detection of antibodies in the plasmonic hotspot of NACHOS, we incorporated the nanoswitch sensing unit in NACHOS containing a 100-nm AgNP as well as in the same DNA origami nanostructure without NPs serving as reference. The efficiency of the nanoswitch opening upon addition of anti-Dig antibodies was then determined analogously to the measurements on the NRO nanosensors (see Figure 2b). In absence of anti-Dig antibodies, nanoswitch openings of 10% and 25% were recorded for the reference structure and NACHOS containing 100-nm Ag NP, respectively (see Figure 2c). The higher level of false positive signals in the NACHOS structure compared to the reference structure can be related to accelerated photobleaching of BBQ650 in the hotspot of plasmonic nanoantennas (Grabenhorst et al., 2020). After 20 min incubation with 100 nM anti-Dig antibodies, nanoswitch opening of 52% and 57% were measured for the reference structure and NACHOS, respectively. This demonstrates a similar accessibility of the nanoswitch for the antibody in the NACHOS structure as in e reference structure and even is comparable to the sterically less complex two-dimensional NRO structure.

Next, we studied the fluorescence enhancement achievable in this single-molecule antibody diagnostic assay. Single-molecule fluorescence transients of the nanoswitch (see Figure 2d and Supplementary Figure 4) were recorded on a confocal microscope for the reference structure and for NACHOS containing AgNPs upon incubation with anti-Dig antibody. Fluorescence enhancement values were calculated by comparing the intensity of the opened nanoswitch (intensity of ATTO 647N) in the NACHOS structure to that of the reference structure. Only transients showing single-step photobleaching were included in the analysis. As shown in Figure 2e, fluorescence enhancement values up to 63-fold were achieved with the NACHOS structure (average fluorescence enhancement 17-fold). These enhancement values could be sufficient to enable the detection of antibodies on the single-molecule level on low-cost optical setups, such as the one based on a monochrome smartphone camera (Trofymchuk et al., 2021, Vietz et al., 2019).

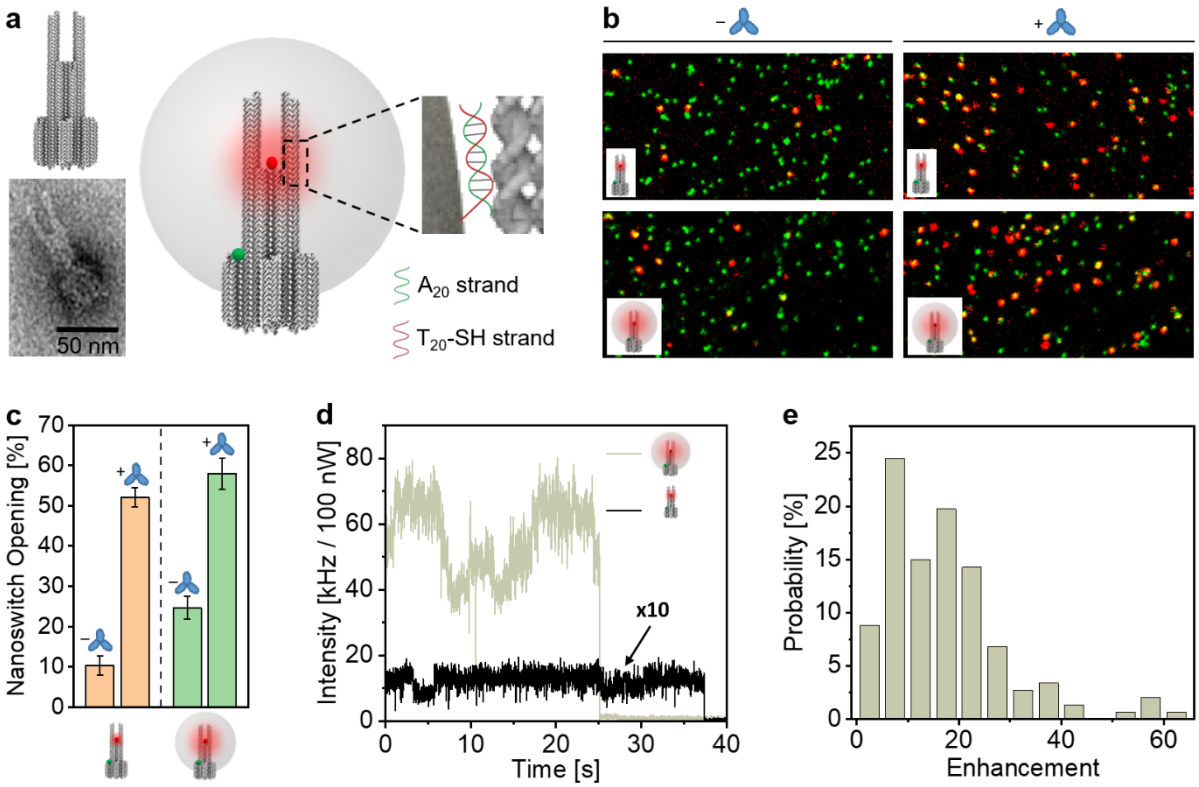

Figure 2. Detection of anti-Dig antibodies with a nanoswitch in the plasmonic hotspot of NACHOS nanostructures with AgNPs. (a) Sketch of the DNA origami structure used for the nanoantenna assembly. A representative class average TEM image of the DNA origami used is shown on the lower left. Schematics of nanoantennas assembly on the right: thiolated DNA-functionalized 100-nm silver nanoparticles are attached to DNA origami nanoantennas via polyadenine (A_{20}) binding strands in zipper-like geometry. (b) Two-color fluorescence confocal images of a reference DNA origami structure without nanoparticles (upper) and with 100-nm silver nanoparticle (lower) before and after 20 min incubation with 100 nM anti-Dig antibodies. The scans show a field of view of 20 µm x 10 µm. (c) Fraction of open nanoswitches quantified by dividing the number of red-green colocalized spots by the total number of all green spots. Over 500 structures from 5 different areas per sample were analyzed. Error bars represent the standard deviation of the 5 areas. (d) Single-molecule fluorescence intensity transients, measured on a confocal microscope, normalized to the same excitation power of a single ATTO 647N dye incorporated in a DNA origami (black) and in a monomer NACHOS structure containing 100-nm AgNP (olive) excited at 639 nm. (e) Fluorescence enhancement distribution of the nanoswitch (ATTO 647 dye) measured in the NACHOS structure. A total number of 113 and 147 reference and NACHOS structures were analyzed, respectively.

Opening kinetics and sensitive concentration range of the nanoswitch on different DNA origami nanostructures

We evaluated the time required to perform the antibody detection assay and the sensitive concentration range of the nanoswitch on the NRO, the reference DNA origami structure without NP and NACHOS containing a 100-nm AgNP. To quantify the kinetics of nanoswitch opening we recorded confocal fluorescence scans of surface immobilized DNA origami nanoswitches before and after different incubation times with 100 nM anti-Dig antibodies (Supplementary Figure 5), while the sensitive detection range was determined by measuring the nanoswitch opening before and after 20 min incubation with different anti-Dig antibody concentrations (Supplementary Figure 6-8). The efficiency of nanoswitch opening was determined for each incubation time (Figure 3a) and each antibody concentration (Figure 3b), respectively. We found that the detection was equally rapid on the different DNA origami structures (for 100 nM anti-Dig antibodies), achieving the highest signal gain after just 5 minutes. This is in

accordance with the fast nanoswitch opening kinetics in solution reported previously (Ranallo et al., 2015).

The target concentration at which the observed signal change is half the maximum signal change (K_D) had values of 129 pM, 800 pM and 1.4 nM for the NRO, the reference DNA origami structure without NP and the NACHOS structure with 100-nm AgNP, respectively. The local environment of the nanoswitch could influence the stability of the open and closed states of the nanoswitch changing the affinity of this sensing unit in different DNA origami designs. Notably, changing the DNA origami structure does provide the means to shift the sensitive concentration range of the antibody detection assay.

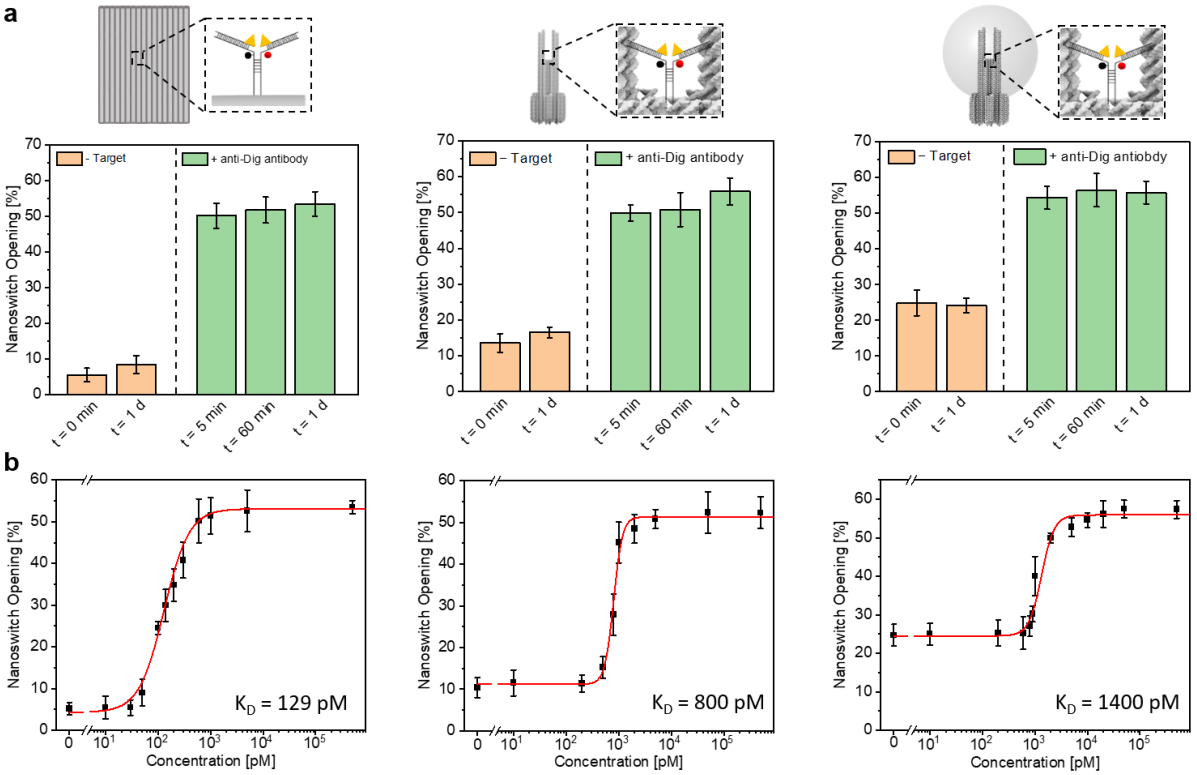

Figure 3. Opening kinetics and sensitive concentration range of the nanoswitch on different DNA origami nanostructures. (a) Nanoswitch opening on the NRO (left), the reference DNA origami structure without nanoparticles (middle) and NACHOS with 100-nm AgNP (right) before and after the incubation with 100 nM anti-Dig antibodies. (b) Nanoswitch opening versus anti-Dig antibody concentration on the NRO (left), the reference DNA origami structure without nanoparticles (middle) and NACHOS with 100-nm AgNP (right). The fraction of opened nanoswitches was quantified from confocal fluorescence scans by dividing the number of red-green colocalized spots by the total number of green spots. Over 300 structures from at least 3 different areas per sample were analyzed. Error bars represent the standard deviation of the areas.

Discussion

Rapidly increasing versatility and complexity of DNA nanostructures together with decrease in cost production of DNA that follows Moore's law (halved every 30 months) (Schmidt et al., 2015) makes them ideal platforms for the development of rapid and

low-cost biosensors. While modular and programmable DNA origami approach has been extensively used for the development of various biosensors its scope of different targets is often limited to nucleic acids. In this work, we report a general strategy how to incorporate the fluorescence-based sensors for antibodies into DNA origami platform. Building on previous work of nanoswitch sensors for antibodies in solution (Ranallo et al., 2015), we showed that these nanoswitch sensors can be successfully incorporated in different DNA origami nanostructures to provide rapid and specific detection of antibodies at the single molecule level. The biorecognition elements of the nanoswitch (antigen or small molecule) were not directly incorporated into the DNA origami design but each anchor was designed to carry complementary DNA sequence to which different biorecognition elements can be bound post synthetically. This flexible and modular nature of this sensing platform allows one to easily extend it to the detection of other antibodies or biomolecular targets. This sensing approach is also not limited to the detection of bivalent binding antibodies as Ricci group has already demonstrated that monovalent binding of two different antibodies could also lead to an opening of the nanoswitch (Ranallo et al., 2015).

On the other hand, the addressability of the DNA origami approach itself opens number of exciting directions as well. In this work, we demonstrated how the modular nature of DNA origami can be used to implement a strategy for signal amplification upon antibody detection, leading to an average fluorescence enhancement of 17-fold. As illustrated recently by detection of single DNA target molecules on a smartphone camera with a help of NACHOS (Trofymchuck et al., 2021), strategies to boost the signal of biomolecular assays could not only help to improve the robustness of biosensing assays but also allow to carry them out on cheap and low-cost devices required for point-of-care applications. An exciting future direction would be to utilize the unprecedented multiplexing capabilities of DNA origami to extend this platform or apply it for highly multiplexed detection of large number of clinically relevant targets. It has, for example, been shown that up to 216 distinct fluorescence barcodes can be implemented on a single DNA origami nanostructure opening exciting opportunities in development of highly multiplexed biosensing strategies (Lin et al., 2012). The nanoswitch sensor platform shown here would allow to combine this multiplexing advantage with specific and sensitive (single molecule level) detection of antibodies on one DNA origami nanostructure.

Limitations of the Study

The single-molecule antibody sensing platform, however, has some limitations as well, especially in the combination of plasmonic signal enhancement by the nanoantenna. One obvious limitation comes from the fact that, the relatively small hotspot size of the DNA nanoantennas (such as NACHOS structure used here), required for high signal enhancement limits the size of the antibody or the biomolecular target that can be detected. Another challenge is related to the photophysics of fluorophore quencher pair – we have recently shown that the photobleaching of the quencher molecule (BBQ650) is accelerated in the hotspot of dimer DNA nanoantennas, leading to an increase of acceptor (ATTO647N) fluorescence even in the absence of the target molecule and giving rise to a false positive signal (Grabenhorst et al., 2020). We also

incorporated the nanoswitch in dimer nanoantennas with two nanoparticles in order to achieve more fluorescence enhancement. For NACHOS with two 100-nm AgNPs we however observed a large number of red-green colocalized spots even before the addition of target antibodies (Supplementary Figure 9), which prevented us from using of this structure for the detection of antibodies. The higher fraction of active red dyes even in the absence of the target molecule and giving rise to false positive signals on the supposedly closed nanoswitch can have different origins. As previously shown (Grabenhorst et al., 2020), the higher excitation power in the dimer hotspot can lead to premature photobleaching of the quencher molecule (BBQ650). Another effect is that quenched dyes are enhanced even more than non-quenched dyes as radiative rates are enhanced by the nanoantennas so that the efficiency of BBQ650 quenching might not be strong enough (Vietz et al., 2017b). We can therefore not conclusively answer the question whether NACHOS would sterically enable antibody binding in the hotspot between two nanoparticles. To this end, multiple and more efficient quencher molecules or replacing the molecular quencher with a small metallic NP might improve the assay. Nevertheless, we believe that the single-molecule DNA origami antibody sensor platform introduced here, presents a useful starting point to further extending the DNA origami sensors beyond the detection of nucleic acids and expanding their scope to antibodies and other sensing applications.

Acknowledgments

Prof. Tim Liedl/Prof. Joachim Rädler (Ludwig-Maximilians-Universität, Department für Physik, Munich, Germany) for providing access to their facilities especially to the transmission electron microscope. Funded by the Deutsche Forschungsgemeinschaft (DFG, German Research Foundation) under Germany`s Excellence Strategy — EXC 2089/1–390776260. P.T. gratefully acknowledges financial support from the DFG (Grant Nos. INST 86/1904-1 FUGG and TI 329/9-2) and BMBF (Grants POCEMON, 13N14336, and SIBOF, 03VP03891. V.G. acknowledge the support by Humboldt Research Fellowships from the Alexander von Humboldt Foundation and European Union`s Horizon 2020 research and innovation program under the Marie Skłodowska-Curie. K.T. acknowledge the support by Humboldt Research Fellowships from the Alexander von Humboldt Foundation. S.R. is supported by European Union's Horizon 2020 research and innovation program under the Marie Skłodowska-Curie grant agreement n. 843179 (''DNA-NANO-AB''). The work was also supported by Associazione Italiana per la Ricerca sul Cancro, AIRC (project n. 21965, F.R.) and by the European Research Council, ERC (Consolidator Grant project n. 819160, F.R.)

Author contributions

M.P., K.T., V.G. and S.R developed the concept of combining the nanoswitch and DNA origami platforms. M.P., K.T., and V.G. prepared samples, performed and analyzed

the measurements. P.T. and F.R. supervised the project. All authors have written, read and approved the final manuscript.

Declaration of interests

P.T. is an inventor on an awarded patent of the described bottom-up method for fluorescence enhancement in molecular assays, EP1260316.1, 2012, US20130252825 A1. The remaining authors declare no competing interests.

STAR Methods

Synthesis of DNA origami

DNA origami structures were designed using the open-source software caDNAno2 (Douglas et al., 2009) and assembled and purified using published protocols (Wagenbauer et al., 2017). For the exact sequences of all unmodified and modified DNA staple strands used to fold the DNA origami structures see Supplementary Table 1 and 2 (NRO) and Supplementary Table 3 and 4 (DNA origami used to build NACHOS). The BBQ650-labelled staple strands were purchased from Biomers.net GmbH (Germany). All other staples were purchased from Eurofins Genomics GmbH (Germany).

For the DNA origami structure used to build NACHOS, 25 µL of p8064 scaffold (produced in-house) at 100 nM were mixed with 18 µL of unmodified staples pooled from 100 µM original concentration and 2 µL of modified staples pooled from 100 µM original concentration. For DNA origami folding, 5 µL of 10x FoB20 folding buffer (200 mM $MgCl_2$, 50 mM Tris, 50 mM NaCl, 10 mM EDTA) were added and the mixture was subjected to a thermal annealing ramp (Supplementary Table 5). Folded DNA origamis were purified from excessive staple strands using 100 kDa Amicon Ultra filters (Merk, Germany) with 6 washing steps with a lower ionic strength buffer (5 mM $MgCl_2$, 5 mM TRIS, 5 mM NaCl, 1 mM EDTA) at 10 krcf for 5 minutes and 20 °C. To extract the purified DNA origamis, the filter was inverted in a new Eppendorf tube and the sample was recovered by spinning for 2 minutes at 1 krcf and 20 °C.

For the NRO, 10 µL of p7249 scaffold (produced in-house) at 100 nM were mixed with 18 µL of unmodified staples pooled from 100 µM original concentration and 4 µL of modified staples pooled from 100 µM original concentration. Briefly, 10 µL of 10x folding buffer (125 mM $MgCl_2$, 400 mM Tris, 200 mM acetic acid, 10 mM EDTA) were added and the mixture was heated to 65 °C in a thermocycler. The solution was kept at this temperature for 15 min before cooling down to 25 °C with a temperature gradient of – 1 °C min^{-1} to finally 25 °C. Samples were purified from excess staple strands by PEG-precipitation. The reaction mixture was mixed 1:1 (v:v) with precipitation buffer (15 % PEG-8000, 10 mM $MgCl_2$, 250 mM NaCl) and spinned at 16 000 g for 45 min at 4 °C. The supernatant was discarded and the pellet was re-dissolved in 100 µL storage buffer (12.5 mM $MgCl_2$, 40 mM Tris, 20 mM acetic acid, 10 mM EDTA). The precipitation procedure was carried out 3 times. Finally, the pellet was dissolved in 20 µL storage buffer.

Functionalization of Silver Nanoparticles

100 nm Ag nanoparticles (100 nm BioPure Silver Nanospheres (Citrate), nanoComposix, USA) were functionalized with polythymidine (T_{20}) ssDNA strands with a thiol modification at the 3'-end (Ella Biotech GmbH, Germany) based on previously described procedures (K. Trofymchuk et al., 2021 and S. Ochmann et al., 2017). For the fabrication of T_{20}-functionalized Ag nanoparticles, 2 mL of 0.025 mg/mL nanoparticle solution in ultra-pure water (Sigma Aldrich, Germany) was heated to 40 °C under permanent stirring at 550 rpm. Briefly, 20 µL of 10% Tween®20 (Thermo Fisher Scientific, USA), 20 µL of a 4:5 (v:v) mixture of 1 M monobasic and dibasic potassium phosphate buffers (P8709 and P8584 Sigma Aldrich, Germany) and 20 µL of a 2 nM polythymidine ssDNA strands (T_{20}-SH-3') were added to the nanoparticle solution and stirred at 40 °C for 1 h. Then, different amounts of 1xPBS buffer (137 mM NaCl, 2.7 mM KCl, 10 mM Na_2HPO_4, 1.8 mM KH_2PO_4) containing 3.3 M NaCl were added stepwise every three minutes to the mixture, until a final concentration of 750 mM NaCl was reached – for the exact salting procedure see Supplementary Table 6. Afterwards, the solution was centrifuged for 12 minutes at 2800 g and 20 °C. The supernatant was discarded and the pellet, in which the particles were concentrated, was re-suspended in PBS10 buffer (147 mM NaCl, 2.7 mM KCl, Na_2HPO_4 10mM, KH_2PO_4 3.9 mM, K_2HPO_4 2.9 mM, 2.5 mM EDTA, 0.01% Tween®20). The washing step was carried out six times. Finally, the nanoparticles were diluted in 1x TE buffer (10 mM Tris, 1 mM EDTA) containing 750 mM NaCl to an absorption of 0.1 (0.1 mm path length) at the excitation maxima on a UV-Vis spectrometer (NanoDrop 2000, Thermo Fisher Scientific, USA).

Transmission electron microscopy (TEM) measurements

TEM grids (Formvar/carbon, 400 mesh, Cu, TedPella, Inc., USA) were Ar-plasma cleaned and incubated with 5 µL of ~ 2-10 nM DNA origami sample for 60 s. Grids were washed with 5 µL 2 % uranyl formate solution and incubated afterwards again with 5 µL 2 % uranyl formate solution for staining. TEM imaging wwas performed on a JOEL JEM-1100 microscope (JEOL GmbH, Japan) with an acceleration voltage of 80 kV.

Sample preparation on the coverslip for single-molecule confocal measurements

Adhesive SecureSeal™ Hybridization Chambers (2.6 mm depth, Grace Bio-Labs, USA) were glued on microscope coverslips of 24 mm × 60mm size and 170 µm thickness (Carl Roth GmbH, Germany). The created wells were incubated with 1 M KOH for 1 h and washed three times with 1× PBS buffer. After surface passivation by incubation with BSA-Biotin (0.5 mg/mL, Sigma Aldrich, USA) for 15 min, the surface was again washed three times with 1× PBS buffer. 100 µL neutravidin (0.25 mg/mL, Sigma Aldrich, USA) was incubated for 10 minutes and then washed three times with 1× PBS buffer. The DNA origami solution was diluted with 1× TE buffer containing 750

mM NaCl to a concentration of ~10-100 pM and then immobilized on the biotin-neutravidin surface via biotin-neutravidin interactions. For this, 100 µL of the DNA origami sample solution was added and incubated for 3 min. Residual unbound DNA origami was removed by washing the wells three times with 1x TE buffer containing 750 mM NaCl. The density of DNA origami on the surface suitable for single-molecule measurements was checked on a confocal microscope. Nanoantenna samples were then incubated with 150 µL of the T20-functionalized AgNPs in 1x TE buffer containing 750 mM NaCl overnight at room temperature. Unbound nanoparticles were removed by washing the samples three times with 1x TE buffer containing 750 mM NaCl. To prevent the evaporation of the samples, wells were glued with tapes. The samples were then imaged either directly or after performing a sensing procedure in 1x TE buffer containing 750 mM NaCl.

Antibody detection assay

For the detection of anti-Dig antibodies, DNA origami bearing a nanoswitch were immobilized on a surface via biotin-neutravidin interactions and nanoparticles were attached to DNA origami samples in analogous way to the previous section. anti-Dig antibodies (Rb Monoclonal, Thermo Fisher Scientific, USA) were diluted to 0.01-500 nM in antibody binding buffer (150 mM NaCl, 50 mM Na_2HPO_4, pH 7). DNA origami samples were incubated with 150 µL of the anti-Dig antibody solution at room temperature before imaging.

Confocal measurements and data analysis

For detection of single-molecule fluorescence, a home-build confocal microscope was used. The setup was based on an inverted microscope (IX-83, Olympus Corportation, Japan) and a 78 MHz-pulsed white light laser (SuperK Extreme EXW-12, NKT Photonics A/S, Denmark) with selected wavelengths of 532 nm and 639 nm. The wavelengths were selected via an acousto-optically tunable filter (AOTF, SuperK Dual AOTF, NKT Photonics A/S, Denmark). This was controlled by a digital controller (AODS 20160 8 R, Crystal Technology, USA) via a computer software (AODS 20160 Control Panel, Crystal Technology, Inc., USA). A second AOTF (AA.AOTF.ns: TN, AA Opto-Electronic, France) was used to alternate 532 nm and 639 nm wavelengths if required, as well as to further spectrally clean the laser beam. It was controlled via home-made LabVIEW software (National Instruments, USA). A neutral density filter was used to regulate the laser intensity, followed by a linear polarizer and a λ/4 plate to obtain circularly polarized excitation. A dichroic beam splitter (ZT532/640rpc, Chroma Technology, USA) and an immersion oil objective (UPlanSApo 100×, NA = 1.4, WD = 0.12 mm, Olympus Corporation, Japan) were used to focus the excitation laser onto the sample. Micropositioning was performed using a Piezo-Stage (P-517.3CL, E-501.00, Physik Instrumente GmbH&Co. KG, Germany). The excitation powers at 639 nm were set to 500 nW for the reference samples and to 100 nW for the nanoantennas for the recording of fluorescence transients. For the confocal scans, 1 µW at 532 nm and 1 µW or 500 nW at 639 nm were used for all samples. Emitted

light was collected by the same objective and filtered from the excitation light by a dichroic beam splitter. The light was later focused on a 50 µm pinhole (Linos AG, Germany) and detected using avalanche photodiodes (SPCM, AQR 14, PerkinElmer, Inc., USA) registered by an TCSPC system (HydraHarp 400, PicoQuant GmbH, Germany) after additional spectral filtering (RazorEdge 647, Semrock Inc., USA for the red channel and BrightLine HC 582/75, Semrock Inc., USA for the green channel). Custom-made LabVIEW software (National Instruments, USA) was used to process the acquired raw data. Background correction was carried out individually for each transient. The extracted data was analyzed in OriginPro2020.

ACUNA, G. P., MOLLER, F. M., HOLZMEISTER, P., BEATER, S., LALKENS, B. & TINNEFELD, P. 2012. Fluorescence enhancement at docking sites of DNA-directed self-assembled nanoantennas. *Science,* 338**,** 506-10.

CHANDRASEKARAN, A. R. 2017. DNA Nanobiosensors: An Outlook on Signal Readout Strategies. *Journal of Nanomaterials,* 2017**,** 2820619.

DASS, M., GÜR, F. N., KOŁĄTAJ, K., URBAN, M. J. & LIEDL, T. 2021. DNA Origami-Enabled Plasmonic Sensing. *The Journal of Physical Chemistry C,* 125**,** 5969-5981.

DOMLJANOVIC, I., CARSTENS, A., OKHOLM, A., KJEMS, J., NIELSEN, C. T., HEEGAARD, N. H. H. & ASTAKHOVA, K. 2017. Complexes of DNA with fluorescent dyes are effective reagents for detection of autoimmune antibodies. *Scientific Reports,* 7**,** 1925.

FUNCK, T., NICOLI, F., KUZYK, A. & LIEDL, T. 2018. Sensing Picomolar Concentrations of RNA Using Switchable Plasmonic Chirality. *Angew Chem Int Ed Engl,* 57**,** 13495-13498.

GODONOGA, M., LIN, T.-Y., OSHIMA, A., SUMITOMO, K., TANG, M. S. L., CHEUNG, Y.-W., KINGHORN, A. B., DIRKZWAGER, R. M., ZHOU, C., KUZUYA, A., TANNER, J. A. & HEDDLE, J. G. 2016. A DNA aptamer recognising a malaria protein biomarker can function as part of a DNA origami assembly. *Scientific Reports,* 6**,** 21266.

GRABENHORST, L., TROFYMCHUK, K., STEINER, F., GLEMBOCKYTE, V. & TINNEFELD, P. 2020. Fluorophore photostability and saturation in the hotspot of DNA origami nanoantennas. *Methods and applications in fluorescence,* 8**,** 024003.

HOLZMEISTER, P., WÜNSCH, B., GIETL, A. & TINNEFELD, P. 2014. Single-molecule photophysics of dark quenchers as non-fluorescent FRET acceptors. *Photochemical & Photobiological Sciences,* 13**,** 853-858.

KE, Y., CASTRO, C. & CHOI, J. H. 2018. Structural DNA Nanotechnology: Artificial Nanostructures for Biomedical Research. *Annual Review of Biomedical Engineering,* 20**,** 375-401.

KE, Y., LINDSAY, S., CHANG, Y., LIU, Y. & YAN, H. 2008. Self-assembled water-soluble nucleic acid probe tiles for label-free RNA hybridization assays. *Science,* 319**,** 180-3.

KEYSER, U. F. 2016. Enhancing nanopore sensing with DNA nanotechnology. *Nature Nanotechnology,* 11**,** 106-108.

KOIRALA, D., SHRESTHA, P., EMURA, T., HIDAKA, K., MANDAL, S., ENDO, M., SUGIYAMA, H. & MAO, H. 2014. Single-Molecule Mechanochemical Sensing Using DNA Origami Nanostructures. *Angewandte Chemie International Edition,* 53**,** 8137-8141.

KUZUYA, A., SAKAI, Y., YAMAZAKI, T., XU, Y. & KOMIYAMA, M. 2011. Nanomechanical DNA origami 'single-molecule beacons' directly imaged by atomic force microscopy. *Nature Communications,* 2**,** 449.

LI, K., STOCKMAN, M. I. & BERGMAN, D. J. 2003. Self-Similar Chain of Metal Nanospheres as an Efficient Nanolens. *Physical Review Letters,* 91**,** 227402.

LI, Z., WANG, L., YAN, H. & LIU, Y. 2012. Effect of DNA Hairpin Loops on the Twist of Planar DNA Origami Tiles. *Langmuir,* 28**,** 1959-1965.

LORETAN, M., DOMLJANOVIC, I., LAKATOS, M., RÜEGG, C. & ACUNA, G. P. 2020. DNA Origami as Emerging Technology for the Engineering of Fluorescent and Plasmonic-Based Biosensors. *Materials,* 13**,** 2185.

NOVOTNY, L. & VAN HULST, N. 2011. Antennas for light. *Nature Photonics,* 5**,** 83-90.

OCHMANN, S. E., VIETZ, C., TROFYMCHUK, K., ACUNA, G. P., LALKENS, B. & TINNEFELD, P. 2017. Optical Nanoantenna for Single Molecule-Based Detection of Zika Virus Nucleic Acids without Molecular Multiplication. *Analytical Chemistry,* 89**,** 13000-13007.

PORCHETTA, A., IPPODRINO, R., MARINI, B., CARUSO, A., CACCURI, F. & RICCI, F. 2018. Programmable Nucleic Acid Nanoswitches for the Rapid, Single-Step Detection of Antibodies in Bodily Fluids. *Journal of the American Chemical Society,* 140**,** 947-953.

PUCHKOVA, A., VIETZ, C., PIBIRI, E., WUNSCH, B., SANZ PAZ, M., ACUNA, G. P. & TINNEFELD, P. 2015. DNA Origami Nanoantennas with over 5000-fold Fluorescence Enhancement and Single-Molecule Detection at 25 muM. *Nano Lett.,* 15**,** 8354-9.

PURCELL E.M. 1946. Proceedings of the American Physical Society. *Physical Review,* 69**,** 674-674.

RANALLO, S., ROSSETTI, M., PLAXCO, K. W., VALLÉE-BÉLISLE, A. & RICCI, F. 2015. A Modular, DNA-Based Beacon for Single-Step Fluorescence Detection of Antibodies and Other Proteins. *Angew Chem Int Ed Engl,* 54**,** 13214-8.

RAVEENDRAN, M., LEE, A. J., SHARMA, R., WÄLTI, C. & ACTIS, P. 2020. Rational design of DNA nanostructures for single molecule biosensing. *Nature Communications,* 11**,** 4384.

RINKER, S., KE, Y., LIU, Y., CHHABRA, R. & YAN, H. 2008. Self-assembled DNA nanostructures for distance-dependent multivalent ligand–protein binding. *Nature Nanotechnology,* 3**,** 418-422.

ROTHEMUND, P. W. K. 2006. Folding DNA to create nanoscale shapes and patterns. *Nature,* 440**,** 297-302.

SCHMIDT, T. L., BELIVEAU, B. J., UCA, Y. O., THEILMANN, M., DA CRUZ, F., WU, C.-T. & SHIH, W. M. 2015. Scalable amplification of strand subsets from chip-synthesized oligonucleotide libraries. *Nature Communications,* 6**,** 8634.

SELNIHHIN, D., SPARVATH, S. M., PREUS, S., BIRKEDAL, V. & ANDERSEN, E. S. 2018. Multifluorophore DNA Origami Beacon as a Biosensing Platform. *ACS Nano,* 12**,** 5699-5708.

SUBRAMANIAN, H. K. K., CHAKRABORTY, B., SHA, R. & SEEMAN, N. C. 2011. The Label-Free Unambiguous Detection and Symbolic Display of Single Nucleotide Polymorphisms on DNA Origami. *Nano Letters,* 11**,** 910-913.

TROFYMCHUK, K., GLEMBOCKYTE, V., GRABENHORST, L., STEINER, F., VIETZ, C., CLOSE, C., PFEIFFER, M., RICHTER, L., SCHÜTTE, M. L., SELBACH, F., YAADAV, R., ZÄHRINGER, J., WEI, Q., OZCAN, A., LALKENS, B., ACUNA, G. P. & TINNEFELD, P. 2021. Addressable nanoantennas with cleared hotspots for single-molecule detection on a portable smartphone microscope. *Nature Communications,* 12**,** 950.

VIETZ, C., KAMINSKA, I., SANZ PAZ, M., TINNEFELD, P. & ACUNA, G. P. 2017a. Broadband Fluorescence Enhancement with Self-Assembled Silver Nanoparticle Optical Antennas. *ACS Nano,* 11**,** 4969-4975.

VIETZ, C., LALKENS, B., ACUNA, G. P. & TINNEFELD, P. 2017b. Synergistic Combination of Unquenching and Plasmonic Fluorescence Enhancement in Fluorogenic Nucleic Acid Hybridization Probes. *Nano Letters,* 17**,** 6496-6500.

VIETZ, C., SCHÜTTE, M. L., WEI, Q., RICHTER, L., LALKENS, B., OZCAN, A., TINNEFELD, P. & ACUNA, G. P. 2019. Benchmarking Smartphone Fluorescence-Based Microscopy with DNA Origami Nanobeads: Reducing the Gap toward Single-Molecule Sensitivity. *ACS Omega,* 4**,** 637-642.

WANG, D., VIETZ, C., SCHRÖDER, T., ACUNA, G., LALKENS, B. & TINNEFELD, P. 2017a. A DNA Walker as a Fluorescence Signal Amplifier. *Nano Letters,* 17**,** 5368-5374.

WANG, P., MEYER, T. A., PAN, V., DUTTA, P. K. & KE, Y. 2017b. The Beauty and Utility of DNA Origami. *Chem,* 2**,** 359-382.

WANG, S., ZHOU, Z., MA, N., YANG, S., LI, K., TENG, C., KE, Y. & TIAN, Y. 2020. DNA Origami-Enabled Biosensors. *Sensors (Basel, Switzerland),* 20**,** 6899.

WOO, S. & ROTHEMUND, P. W. 2011. Programmable molecular recognition based on the geometry of DNA nanostructures. *Nat Chem,* 3**,** 620-7.

ZHANG, Z., WANG, Y., FAN, C., LI, C., LI, Y., QIAN, L., FU, Y., SHI, Y., HU, J. & HE, L. 2010a. Asymmetric DNA Origami for Spatially Addressable and Index-Free Solution-Phase DNA Chips. *Advanced Materials,* 22**,** 2672-2675.

ZHANG, Z., ZENG, D., MA, H., FENG, G., HU, J., HE, L., LI, C. & FAN, C. 2010b. A DNA-Origami chip platform for label-free SNP genotyping using toehold-mediated strand displacement. *Small,* 6**,** 1854-8.